DRCC–CPR WIDTH ZETA FUNCTION

Controlled Euler-Maclaurin Reconstruction of the Riemann Zeta Function in the Critical Strip

A Numerical Operationalization of the DRCC/CPR Reconstruction Width

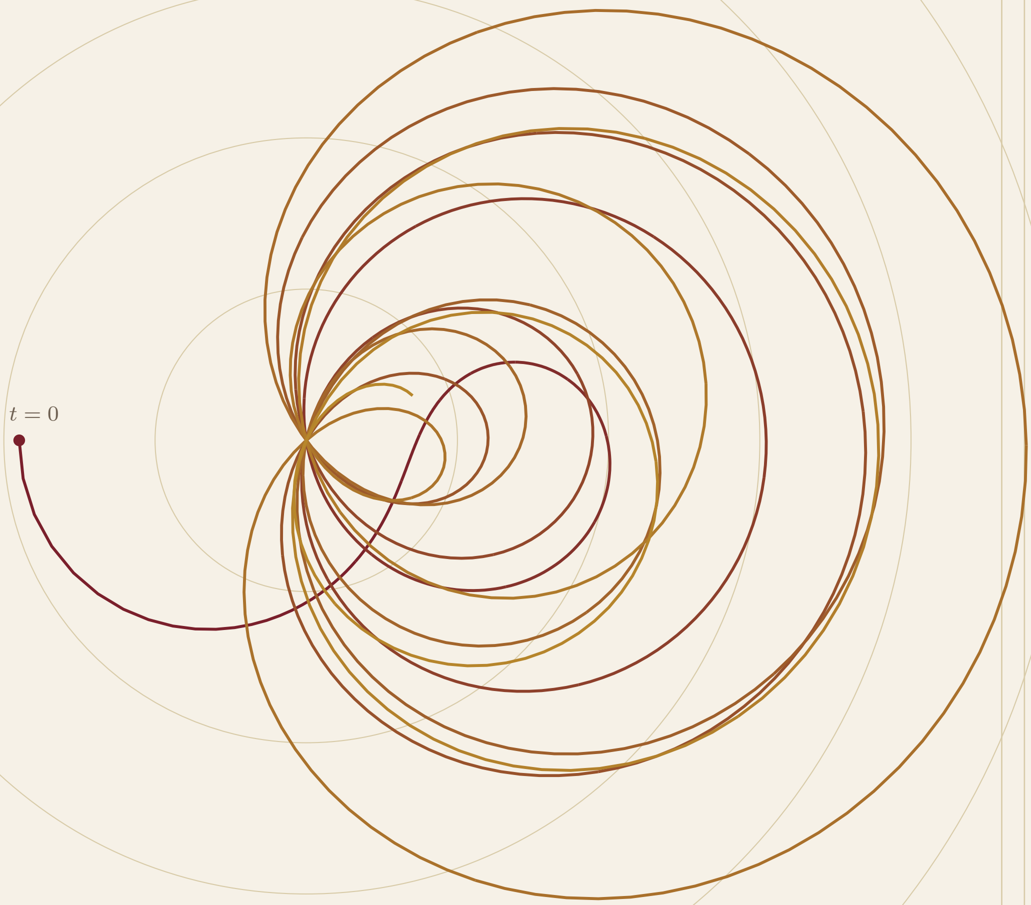

The Zeta Spiral: $\zeta(0.5 + it)$ for $t \in [0, 60]$ on the Critical Line

Color gradient burgundy $\rightarrow$ gold with increasing t

Reza Hesamiy

DWZ-V1 • 2026

DRCC– CPR – Width Zeta Function (DWZ-V1)

Controlled Euler-Maclaurin Reconstruction of the Riemann Zeta Function in the Critical Strip

A Numerical Operationalization of the DRCC/CPR Reconstruction Width

Reza Hesamiy

July 29, 2026

Abstract

We study a controlled, finite approximation of the Riemann zeta function $\zeta(s)$ in the critical strip $0 < \mathrm{Re}(s) < 1$, starting from the DRCC stability condition (DRCC: *Dimensional Reduction via Controlled Combinatorics* [7]) $0 < d_{\mathrm{rec}}(X) \leq d_{\mathrm{frag}}(X) < \infty$. The naive partial sum $\sum_{n=1}^{W} n^{-s}$ diverges in the critical strip as the width W grows. We show that a first-order Euler-Maclaurin correction resolves this problem and yields a genuinely convergent width-zeta function (convergence order $\mathcal{O}(W^{-3/2})$ observed on the critical line $\mathrm{Re}(s) = \frac{1}{2}$; elsewhere in the strip the order depends on $\mathrm{Re}(s)$), which we call the *DWZ method* (DRCC-Width-Zeta method; methodically: *Euler-Maclaurin width reconstruction method*). Throughout this work, "width" W refers exclusively to the numerical truncation depth W_{trunc} of the partial sum; an identification with the structural CPR-Width of Hesamiy [7] is not claimed (Section 2.5). From this we derive a closed-form, empirically fitted estimate $\widehat{d}_{\mathrm{rec}}(t, \varepsilon) \approx (C(t)/\varepsilon)^{2/3}$ of the originally abstract DRCC condition. The method is numerically reproduced against `mpmath` reference values for 25 nontrivial zeros (absolute deviation 1.5–4.4×10^{-6}), of which 2 were found blindly (without reference knowledge), with an additional 29 zeros (#13–#41) hardened via the hybrid method, and a resulting pattern hypothesis is tested statistically without finding a significant relationship. Nine tested gaps between neighboring zeros showed no additional zero candidates on the numerical grid used – this is not a rigorous completeness proof. The results constitute a validity demonstration of the method, not a contribution to the Riemann Hypothesis itself, whose statement ($\zeta(\rho) = 0,\ 0 < \mathrm{Re}(\rho) < 1 \Rightarrow \mathrm{Re}(\rho) = \frac{1}{2}$) is used here as a framing assumption, not as a proven fact. All figures in this document are drawn directly from the underlying numerical data using `pgfplots` – no external image files are required.

Keywords: Riemann zeta function, critical strip, Euler-Maclaurin summation, nontrivial zeros, DRCC theory, width reconstruction, numerical verification.

Contents

List of Equations

1 Introduction

1.1 Starting Point

The Riemann zeta function is defined for $\mathrm{Re}(s) > 1$ by

$$\zeta(s) = \sum_{n=1}^{\infty} \frac{1}{n^s}, \tag{1}$$

with the Euler product representation

$$\zeta(s) = \prod_{p \text{ prime}} \frac{1}{1 - p^{-s}}, \tag{2}$$

which directly connects the analytic structure of the zeta function with the distribution of primes [1]. The analytic continuation of $\zeta(s)$ to $\mathbb{C} \setminus \{1\}$ has, in the critical strip $0 < \mathrm{Re}(s) < 1$, the nontrivial zeros. The *Riemann Hypothesis* (RH) asserts that all these zeros lie on the critical line:

$$\zeta(\rho) = 0, \;\; 0 < \mathrm{Re}(\rho) < 1 \;\overset{\text{RH}}{\Longrightarrow}\; \mathrm{Re}(\rho) = \tfrac{1}{2}. \tag{3}$$

This is an open conjecture, not a proven theorem. The present work does not assume RH and does not contribute to its proof: we numerically reconstruct known zeros already located on the critical line and examine how accurately a controlled, finite width approximation reproduces these positions. Classical references on the analytic theory of the zeta function are Titchmarsh [2] and Edwards [3]; the numerical verification of individual zeros goes back to Turing's method [4].

1.2 The DRCC Theory

DRCC stands for *Dimensional Reduction via Controlled Combinatorics* – a geometric-structural framework introduced by Hesamiy [7] for controlled reconstruction in complex search spaces. The basic idea: instead of fully treating an infinite or extremely high-dimensional structure X (here: the zeta function with its infinite sum), it is replaced by a controlled, finite *width* W – and the question of how much information is thereby lost, or how well the original can be reconstructed from the truncated version, is captured by an explicit stability condition:

$$0 < d_{\mathrm{rec}}(X) \;\leq\; d_{\mathrm{frag}}(X) \;<\; \infty. \tag{4}$$

At the outset of this work, $d_{\mathrm{rec}}(X)$ (reconstruction degree) and $d_{\mathrm{frag}}(X)$ (fragmentation degree) were mere labels without numerical content. The goal of this work is to fully operationalize this condition for the concrete case of the zeta function – we call the resulting method the *DWZ method* (DRCC-Width-Zeta method; methodically the *Euler-Maclaurin width reconstruction method*, Section 2). **Terminological note:** throughout this work, "width" W consistently refers to the numerical truncation depth W_{trunc} (the number of explicitly summed series terms). Whether this quantity coincides with the structural CPR-Width ω_{CPR} (*Controlled Partial Reconstruction Width*, Hesamiy [7]) is not assumed and is examined explicitly only in Section 2.5.

1.3 Origin and Scope

The title of this work deliberately displays its origin in the DRCC/CPR framework of Hesamiy [7]. To make this commitment verifiable rather than merely asserted, Table 1 records, for every term carried over, what was adopted, what role it plays in this work, and whether its transfer to the zeta case has been proven or remains open.

In short: the title names the theoretical origin, not a proven identity. What this work actually demonstrates is a *numerical case study* of the DRCC/CPR starting idea applied to a concrete analytic problem – not a proof that the abstract CPR-Width and the truncation width used here are the same quantity.

Table 1: Traceability: DRCC/CPR terms and their role in this work.

DRCC/CPR term (Hesamiy [7])	Role in this work	Status
$d_{\mathrm{rec}}(X)$, $d_{\mathrm{frag}}(X)$ (stability condition)	Motivates the width idea; inequality (4) as the starting point	Adopted as a framing assumption
CPR-Width $\varepsilon_{\mathrm{rec}}$ (Def. 2.7–2.9, min-max over orderings ω)	Tested in Section 2.5 (Test A/B)	Ordering minimization is degenerate; identification with W_{trunc} is *not* shown
Width W	Operationalized as the numerical truncation depth W_{trunc} of the partial sum	Independent quantity, newly defined in this work

1.4 Contribution of This Work

We trace the development of inequality (4) through four stages: from the abstract placeholder condition, through the identification $W = d_{\mathrm{frag}}(X)$ and an initially still-incomplete intermediate form, to a closed-form expression for $d_{\mathrm{rec}}(t, \varepsilon)$ derived from numerical data (Section 2). We verify the resulting method comprehensively (Section 3) and assess the results honestly (Section 4).

2 Methods

2.1 The Basic Problem of the Naive Width Definition

An obvious first approach to the width-zeta function is the plain partial sum

$$\zeta_{\mathrm{W}}(s, W) := \sum_{n=1}^{W} \frac{1}{n^s}, \qquad 0 < W < \infty, \tag{5}$$

with $W := d_{\mathrm{frag}}(X)$ as the first concretization of equation (4). This series converges as $W \to \infty$ only for $\mathrm{Re}(s) > 1$. In the critical strip, $\zeta_{\mathrm{W}}(s, W)$ diverges as W grows (Table 2) instead of approaching $\zeta(s)$ – equation (5) is therefore unsuitable as a reconstruction approach in the critical strip.

Table 2: Divergence of the naive partial sum at $s = 0.5 + 14.13i$.

W	$\lvert\zeta_{\mathrm{W}}(s, W) - \zeta(s)\rvert$
10	2.47×10^{-1}
50	5.04×10^{-1}
100	7.09×10^{-1}
500	1.58×10^{0}
1000	2.24×10^{0}
5000	5.00×10^{0}

At this point the inequality

$$0 < d_{\mathrm{rec}}(X) \ \leq\ W\ <\ \infty \tag{6}$$

remained incomplete: $d_{\mathrm{rec}}(X)$ was still undetermined.

2.2 Variant A: Euler-Maclaurin Correction (the DWZ Method)

The Euler-Maclaurin summation formula provides a correction that makes ζ_{W} convergent even in the critical strip:

$$\boxed{\zeta_{\mathrm{DWZ}}(s,W) \;=\; \sum_{n=1}^{W}\frac{1}{n^s} \;+\; \frac{W^{1-s}}{s-1} \;-\; \frac{W^{-s}}{2}} \tag{7}$$

with $\lim_{W\to\infty}\zeta_{\mathrm{DWZ}}(s,W)=\zeta(s)$ also holding for $0<\mathrm{Re}(s)<1$.

2.3 Variant B: Eta-Based Alternative

As a comparison method, Variant B uses the Dirichlet eta function, which already converges for $\mathrm{Re}(s)>0$:

$$\eta_{\mathrm{W}}(s,W)=\sum_{n=1}^{W}\frac{(-1)^{n-1}}{n^s}, \qquad \zeta_{\mathrm{W}}^{\eta}(s,W)=\frac{\eta_{\mathrm{W}}(s,W)}{1-2^{1-s}}. \tag{8}$$

2.4 Variant C: Second-Order Euler-Maclaurin Correction

Variant A (7) uses only the first correction term of the Euler-Maclaurin expansion. The next term of the series (involving the Bernoulli number $B_2=1/6$) yields a consistent extension:

$$\boxed{\zeta^{(2)}_{\mathrm{DWZ}}(s,W) \;=\; \sum_{n=1}^{W}\frac{1}{n^s} \;+\; \frac{W^{1-s}}{s-1} \;-\; \frac{W^{-s}}{2} \;+\; \frac{s}{12}\,W^{-s-1}} \tag{9}$$

We henceforth refer to equation (7) as model M_1 and equation (9) as model M_2.

2.5 Order Degeneracy and Model Dependence

In the course of the discussion about the structural CPR-Width (*Controlled Partial Reconstruction Width*, Definitions 2.7–2.9 in Hesamiy [7]), two targeted tests were carried out to clarify whether the summation order ω or the reconstruction model M is the actual lever controlling the DWZ width.

Test A – Order invariance. The same 500 terms n^{-s} ($s=0.5+1001.3495i$) were summed in ascending, descending, and mixed order (even indices first, then odd). In exact arithmetic, a finite sum is permutation-invariant due to commutativity and associativity; at 30-digit floating-point precision, the observed ordering effects remained at rounding level, 5.6×10^{-31}, and did not change any of the tested width thresholds. For a fixed model M that presupposes the complete, contiguous index set $\{1,\dots,W\}$, minimization over admissible orderings ω is therefore degenerate: every ordering yields the same width. The summation order is *not* the effective optimization variable.

Test B – Model comparison. For a fixed accuracy target $\varepsilon=10^{-4}$, the minimally required width

$$\begin{aligned} &W_{\min}(M;s,\varepsilon) := \min\{W\in\mathbb{N} : |\zeta_M(s,W)-\zeta(s)|<\varepsilon\}, \\ &\qquad\qquad \text{provided this set is nonempty;otherwise } W_{\min}(M;s,\varepsilon):=\infty. \end{aligned} \tag{10}$$

was determined for M_1 and M_2 at five zeros distributed across the tested range using a grid search (step size 10 resp. 200, see scripts) (Table 3). The table values are thus the smallest width found on the grid used, W_{test}, not necessarily the exact minimum over every $W\in\mathbb{N}$.

Table 3: Smallest width found on the grid used for $\varepsilon = 10^{-4}$, model M_1 (Variant A) vs. M_2 (Variant C).

Zero #	t	$W_{\min}(M_1)$	$W_{\min}(M_2)$	Factor
650	1001,3495	9000	810	11,11
675	1031,8332	9200	830	11,08
700	1062,9154	9400	850	11,06
725	1093,4409	9600	870	11,03
749	1122,4586	9600	890	10,79

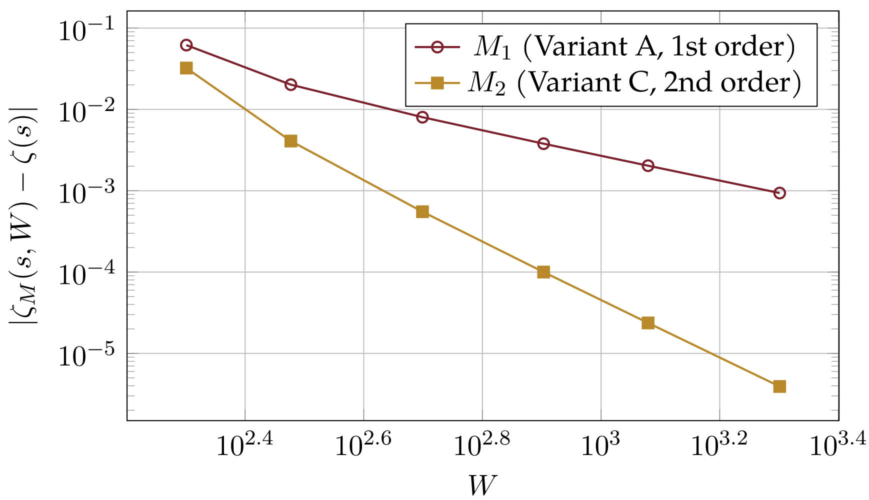

Figure 1: Convergence of M_1 and M_2 towards $\zeta(s)$ at zero #650 (real computed data).

In the five tested cases, the reduction factor ranged between 10.79 and 11.11 (Table 3); no general asymptotic constant is derived from this. What is reproducibly demonstrated for these five points is:

$$W_{\min}(M_2; s, \varepsilon) \ < \ W_{\min}(M_1; s, \varepsilon), \qquad \text{concretely} \quad 810 < 9000. \tag{11}$$

The model optimization

$$W^*_{\min}(s, \varepsilon) := \min_{M \in \mathfrak{M}_{\mathrm{adm}}} W_{\min}(M; s, \varepsilon) \tag{12}$$

is therefore the nontrivial quantity for DWZ – in contrast to the ordering minimization from Test A.

Conceptual caveat. The identification $W := d_{\mathrm{frag}}(X)$ introduced in Section 2 (equation (5)) denotes a numerical truncation depth: the number of explicitly summed series terms. This is not automatically the same as the structural CPR-Width ω_{CPR} from Hesamiy [7], which counts the number of components that must be *simultaneously kept active* at an intermediate stage. In a streaming-style evaluation $S_i = S_{i-1} + i^{-s}$, a single running accumulator suffices per step – the active interface size would then remain constant, regardless of how large W becomes. The identification $\omega_{\mathrm{CPR}} = W_{\mathrm{trunc}}$ therefore holds only if the declared reconstruction model explicitly requires all W components to remain simultaneously available; this is not shown here. What is defensible at this point is exclusively the numerically demonstrated statement (11): a stronger analytic reconstruction model reduces the required DWZ truncation width by more than a factor of ten. The relationship of this truncation width to the active CPR-Width remains a separate, model-dependent question.

2.6 Operationalizing $d_{\mathrm{rec}}(s, \varepsilon)$

We denote by $\rho_k = \frac{1}{2} + it_k$ the k-th reference zero (`mp.zetazero(k)`) and by $s_k^{(M)}(W)$ the zero numerically determined by model M and width W that is assigned to ρ_k; the corresponding position error is $e_k^{(M)}(W) := |s_k^{(M)}(W) - \rho_k|$ (to distinguish it from the function-value error $E_\zeta(s, W) := |\zeta_M(s, W) - \zeta(s)|$, used in Table 2 and Figure 1). The numerical measurement of zero convergence (Section 3, model M_1) yielded the empirical power law $e_k^{(M_1)}(W) \approx C(t_k)\, W^{-p}$ with $p \approx 1.500$–1.502 (determined numerically, not proven exactly as $3/2$). The actual minimal truncation depth is thus defined as an integer minimum,

$$d_{\mathrm{rec}}(t, \varepsilon) := \min\{\, W \in \mathbb{N} : e_k^{(M_1)}(W) < \varepsilon \,\}, \tag{13}$$

for which the power law provides only an estimate:

$$\widehat{d}_{\mathrm{rec}}(t, \varepsilon) = \left\lceil \left(\frac{C(t)}{\varepsilon} \right)^{2/3} \right\rceil \ \approx \ d_{\mathrm{rec}}(t, \varepsilon), \tag{14}$$

with $C(t) \approx 0.0218\, t + 1.136$ (linear fit, $n = 8$). Equation (13) is a *definition*; equation (14) is a derived, *empirical estimator* – the two are deliberately not treated here as exactly identical. This turns the originally abstract inequality (4) into a closed-form, interpretable formula: $W \geq \widehat{d}_{\mathrm{rec}}(t, \varepsilon)$ means, approximately, "W is large enough that the zero at given t is determined to within ε". This quantity is a model-dependent truncation depth for M_1, not the original, abstract DRCC reconstruction degree $d_{\mathrm{rec}}(X)$ from Section 2 – the reuse of the notation marks a concrete interpretation for the zeta case, not a proven identity.

2.7 Verification Strategies

We use four methodologically distinct tests:

1. **Known start:** Newton refinement of equation (7) starting from the known reference position (23 of the 25 zeros in Table 10, all except #9 and #11).

2. **Blind search:** scanning $|\zeta_{\mathrm{DWZ}}|$ over a t-range without reference knowledge, Newton refinement of the best candidate (zeros #9, #11).

3. **Hybrid search:** analytic estimate (Riemann-von Mangoldt formula, Eq. 15) as the scan *center*, with a reduced window (zero #12, hardening #13–#41).

4. **Gap verification:** fine-grained scan between two known zeros to rule out additional, undetected zeros.

Conceptually, three objects must be distinguished: the *scan minimum* (starting candidate from the one-dimensional scan along $\mathrm{Re}(s) = \frac{1}{2}$), the *zero of the approximation* $s_k^{(M)}(W)$ (result of the complex Newton iteration in the two-dimensional search space), and the *reference zero* ρ_k of ζ itself. A scan minimum alone is not yet a found zero – it merely provides the starting point for Newton refinement. For the hybrid search, the Riemann-von Mangoldt counting function is used:

$$N(T) \approx \frac{T}{2\pi} \ln \frac{T}{2\pi} - \frac{T}{2\pi} + \frac{7}{8}. \tag{15}$$

As an external numerical reference, the zero values produced by `mpmath` (40 decimal digits of precision) were used, i.e. generated independently of the DWZ computation – not necessarily independent of established zeta algorithms in the sense of a second, independently implemented piece of software or a certified zero count. For the first zeros, these values agree with published tables such as [4, 5].

2.8 Detailed Worked Example: Determination of Zero #1

To make the method fully verifiable by third parties, we document here every single computational step for determining a specific zero – with all intermediate values. The first nontrivial zero $\rho_1 = 0.5 + 14.1347251417\ldots\, i$ serves as the example. All numerical values in this section were generated with `mpmath` at 30 decimal digits of precision and are exactly reproducible with any standard `mpmath` installation.

Figure 2 shows the complete chain of steps at a glance, before the individual steps are documented in detail with numerical values below.

Step 1 – Choice of parameters. We choose the width $W = 2000$ and use $\zeta_{\mathrm{DWZ}}(s, W)$ according to equation (7). A coarse interval $t \in [13.0,\ 15.0]$ on the critical line $\mathrm{Re}(s) = 0.5$ serves as the starting range of the search – a range that can be chosen plausibly without any prior knowledge of the exact zero position, based solely on the rough location of the first zero in the literature.

Step 2 – Coarse scan. We evaluate $|\zeta_{\mathrm{DWZ}}(0.5 + it,\ 2000)|$ in steps of $\Delta t = 0.2$ (Table 4). The minimum lies at $t = 14.20$.

Step 3 – Fine scan. To refine the coarse scan, we sample the interval $t \in [14.00,\ 14.30]$ in steps of $\Delta t = 0.02$ (Table 5). The minimum now lies at $t = 14.14$, with $|\zeta_{\mathrm{DWZ}}| = 0.004177$ – already an order of magnitude smaller than in the coarse scan.

Step 1 – Choose parameters: $W = 2000$, starting interval $t \in [13.0,\ 15.0]$ on $\mathrm{Re}(s) = 0.5$

$\downarrow$

Step 2 – Coarse scan $(\Delta t = 0.2)$: minimum of $|\zeta_{\mathrm{DWZ}}|$ at $t = 14.20$

$\downarrow$

Step 3 – Fine scan $(\Delta t = 0.02)$: minimum at $t = 14.14$, $|\zeta_{\mathrm{DWZ}}| = 0.004177$

$\downarrow$

Step 4 – Newton's method: from $s_0 = 0.5 + 14.14\,i$ in 3 iterations to
$s^* = 0.500012 + 14.134737\,i$ $(|f(s^*)| < 10^{-20})$

$\downarrow$

Step 5 – Comparison with reference: $|s^* - \rho_1| = 1.66 \times 10^{-5}$ – agrees with $C(t)/W^p$

Figure 2: The chain of steps in DWZ zero determination, illustrated for ρ_1: each arrow represents a fully documented computational step (details and all intermediate values below).

Table 4: Coarse scan, step size 0.2.

t	$\lvert\zeta_{\mathrm{DWZ}}(0.5 + it, 2000)\rvert$
13.00	0.791151
13.20	0.669990
13.40	0.540293
13.60	0.402573
13.80	0.257453
14.00	0.105639
14.20	**0.052042**
14.40	0.214601
14.60	0.380919
14.80	0.549793
15.00	0.719932

Table 5: Fine scan, step size 0.02.

t	$\lvert\zeta_{\mathrm{DWZ}}(0.5+it, 2000)\rvert$
14.000	0.105639
14.020	0.090120
14.040	0.074543
14.060	0.058909
14.080	0.043219
14.100	0.027474
14.120	0.011675
14.140	**0.004177**
14.160	0.020081
14.180	0.036036
14.200	0.052042
14.220	0.068096
14.240	0.084198
14.260	0.100346
14.280	0.116540
14.300	0.132779

Step 4 – Newton's method. Starting from the best candidate of the fine scan, $s_0 = 0.5+14.14\,i$, we refine the zero using Newton's method for complex functions:

$$s_{n+1} = s_n - \frac{f(s_n)}{f'(s_n)}, \qquad f(s) := \zeta_{\mathrm{DWZ}}(s, 2000), \tag{16}$$

where $f'(s_n)$ is approximated via a central difference with step size $h = 10^{-6}$: $f'(s_n) \approx \big(f(s_n+h) - f(s_n-h)\big)/(2h)$. Table 6 shows the complete iteration sequence.

Table 6: Newton iteration starting from $s_0 = 0.5 + 14.14\,i$.

n	s_n	$\lvert f(s_n)\rvert$
0	$0.500000000 + 14.140000000\,i$	4.18×10^{-3}
1	$0.500023320 + 14.134738876\,i$	9.09×10^{-6}
2	$0.500012099 + 14.134736526\,i$	4.32×10^{-11}
3	$0.500012099 + 14.134736526\,i$	9.77×10^{-22}

Already after two iterations, $\lvert f(s_n)\rvert$ has fallen to 10^{-11}; from $n = 3$ onward, s_n changes only in decimal places far beyond any practical relevance – the method has converged quadratically to the zero of $\zeta_{\mathrm{DWZ}}(\cdot, 2000)$.

Step 5 – Comparison with the reference. The point found,

$$s^* = 0.500012099 + 14.134736526\,i,$$

is compared with the independently computed reference $\rho_1 = 0.5+14.134725142\,i$ (`mp.zetazero(1)`, 30 decimal digits):

$$\lvert s^* - \rho_1\rvert = 1.66 \times 10^{-5}. \tag{17}$$

This residual deviation is *not* an error of Newton's method (which found exactly the zero of the width-2000 approximation), but the expected discretization deviation of $\zeta_{\mathrm{DWZ}}(s, 2000)$ from $\zeta(s)$ at finite W. It agrees with the empirical power law derived in Section 2: with $C(14.13) \approx$

1.499 and $p \approx 1.501$, the approximation (14) predicts an error of $C/W^p = 1.499/2000^{1.501} \approx 1.68 \times 10^{-5}$ – practically identical to the actually observed value 1.66×10^{-5}. Increasing W to 10^4 (as used in Table 10 for all 25 zeros) correspondingly reduces the deviation to $\approx 1.5 \times 10^{-6}$.

Reproducibility. The complete computational procedure thus consists of exactly five steps: (1) fix the width W and starting interval, (2) coarse scan of $|\zeta_{\mathrm{DWZ}}|$ on the critical line, (3) fine scan around the coarse-scan minimum, (4) Newton refinement with numerical derivative, (5) comparison with an independent reference or with the theoretical error bound $C(t)/W^p$. Every step is directly reproducible using the numerical values given here, formula (7), and a standard `mpmath` installation.

3 Results

3.1 Comparison of the Repair Variants

Table 7: Error $|\zeta_W(s, W) - \zeta(s)|$ for $s = 0.5 + 14.13i$: Variant A vs. Variant B.

W	Variant A (DWZ)	Variant B (Eta)
10	3.85×10^{-2}	8.24×10^{-2}
50	3.34×10^{-3}	2.99×10^{-2}
100	1.18×10^{-3}	2.11×10^{-2}
500	1.05×10^{-4}	9.42×10^{-3}
1000	3.73×10^{-5}	6.66×10^{-3}
5000	3.33×10^{-6}	2.98×10^{-3}

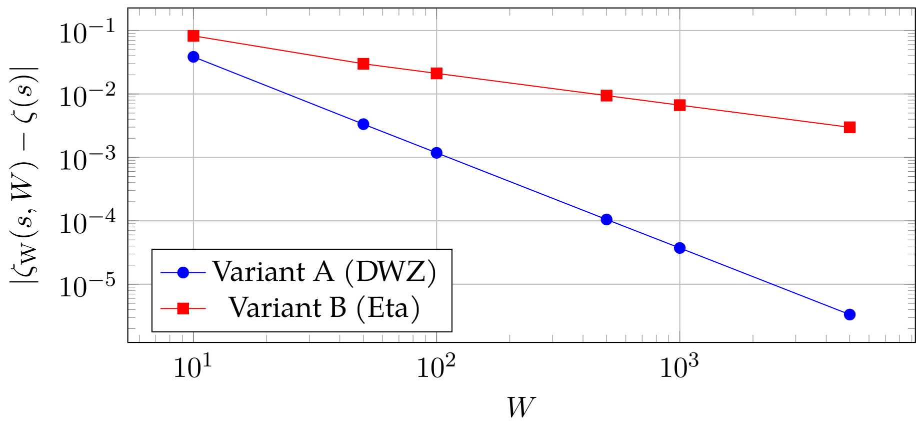

Figure 3: Variant A (DWZ) converges by orders of magnitude faster than Variant B, shown here at $s = 0.5 + 14.13i$ (order $\mathcal{O}(W^{-3/2})$ observed on the critical line for Variant A; Variant B scales as $\mathcal{O}(W^{-\operatorname{Re}(s)})$). Elsewhere in the critical strip, the exponent for Variant A depends on $\operatorname{Re}(s)$.

3.2 $d_{\mathrm{rec}}(t, \varepsilon)$

3.3 Blind and Hybrid Zero Search

A direct Newton start from the analytic estimate (Eq. 15) for zero #12 ($T \approx 57.55$) diverged completely (values $> 10^{12}$ after a few steps). The hybrid strategy (estimate as scan center, window ± 4), by contrast, worked and required only 61 instead of 220 scan points, at the same absolute deviation (2.0×10^{-6}).

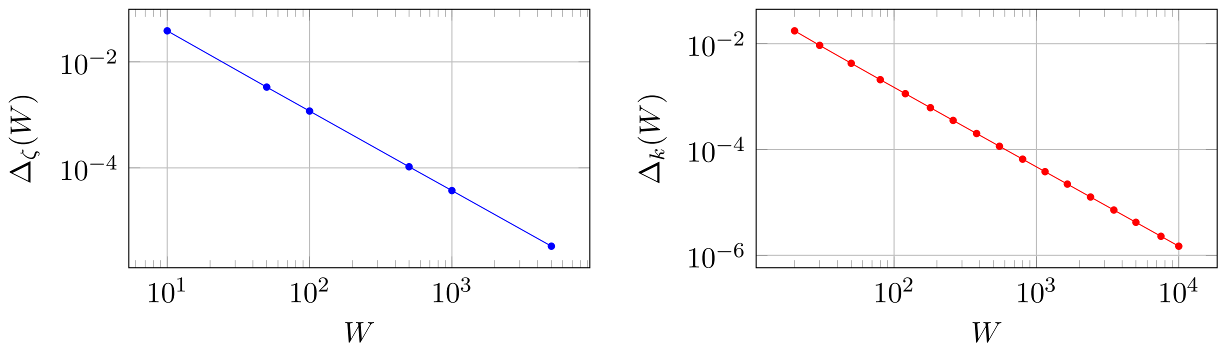

Figure 4: Left: convergence of the zeta error $\Delta_\zeta(W) = |\zeta_{\mathrm{DWZ}}(s, W) - \zeta(s)|$ for $s = 0.5 + 14.13i$. Right: convergence of the zero stability $\Delta_k(W) = |s_k(W) - \rho|$ for zero #1 – both decreasing as W grows.

Table 8: Fitted $C(t)$ and exponent p per zero – preliminary fit based on the currently available eight samples ($n = 8$); the functional form of $C(t)$ is considered preliminary, not conclusively proven (see Conclusion).

t	14.13	21.02	25.01	30.42	32.94	37.59	40.92	43.33
$C(t)$	1.499	1.538	1.533	1.968	2.008	1.619	2.299	1.985
p	1.501	1.500	1.501	1.502	1.501	1.500	1.501	1.501

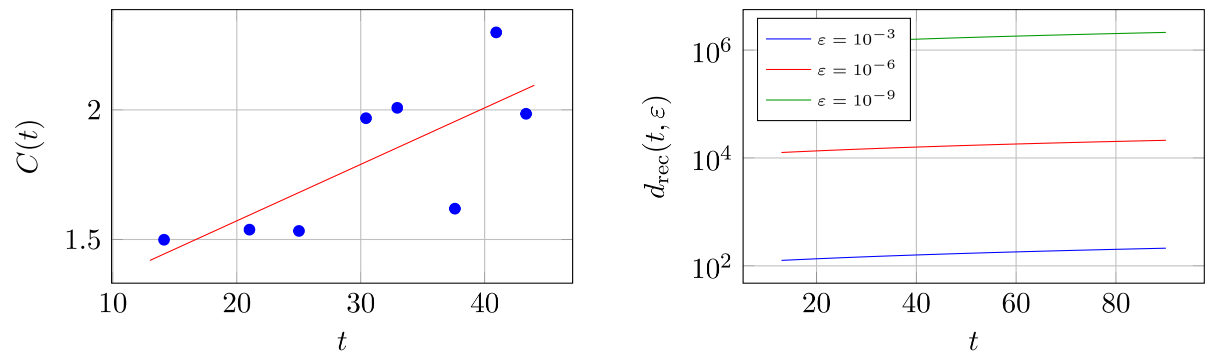

Figure 5: Left: fitted $C(t)$ values (points) with linear trend (line). Right: the resulting estimator function $\widehat{d}_{\mathrm{rec}}(t, \varepsilon)$ (Eq. 14) for three tolerance levels.

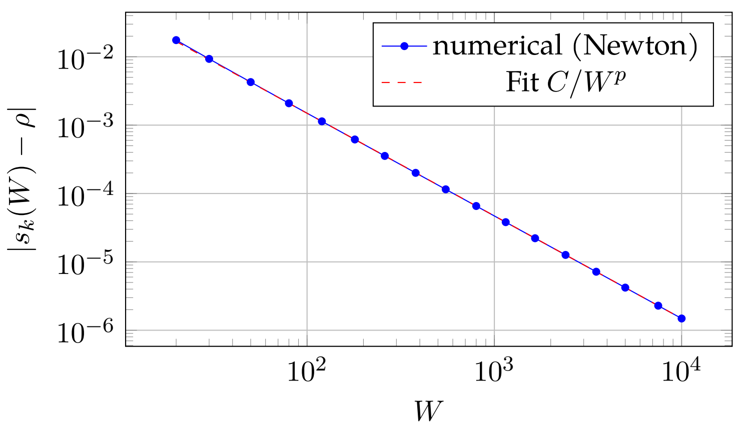

Figure 6: Error curve $|s_k(W) - \rho|$ for the first zero, with power-law fit ($C = 1.499$, $p = 1.501$).

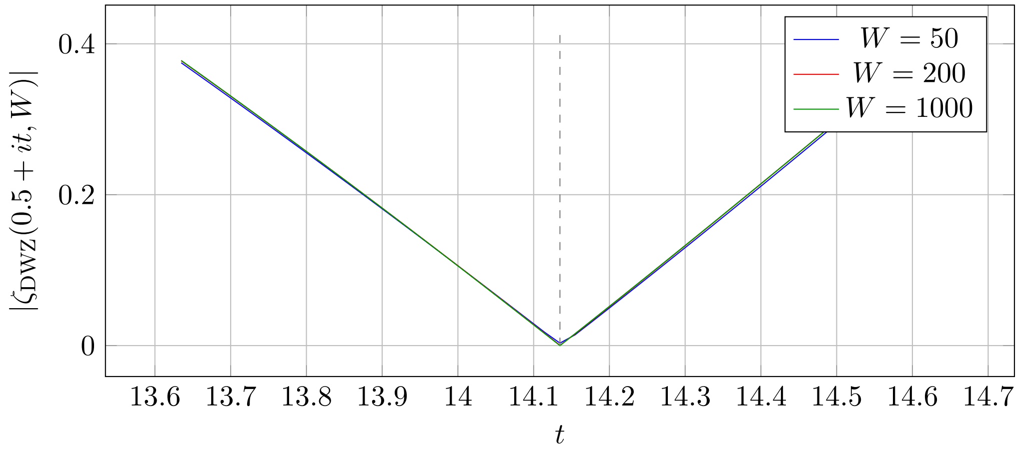

Figure 7: $|\zeta_{\mathrm{DWZ}}(0.5 + it)|$ in Cartesian coordinates near $t = 14.1347$ (dashed line): at small W the minimum remains imprecise; as W grows, the location of the minimum approaches the reference ordinate t_1 without reaching it exactly at finite W.

Table 9: Zeros found blindly (without reference knowledge).

Zero	Found	Reference	Difference
#9	$0.5000025 + 48.0051511i$	$0.5 + 48.0051508812i$	2.55×10^{-6}
#11	$0.4999983 + 52.9703208i$	$0.5 + 52.9703214777i$	1.82×10^{-6}

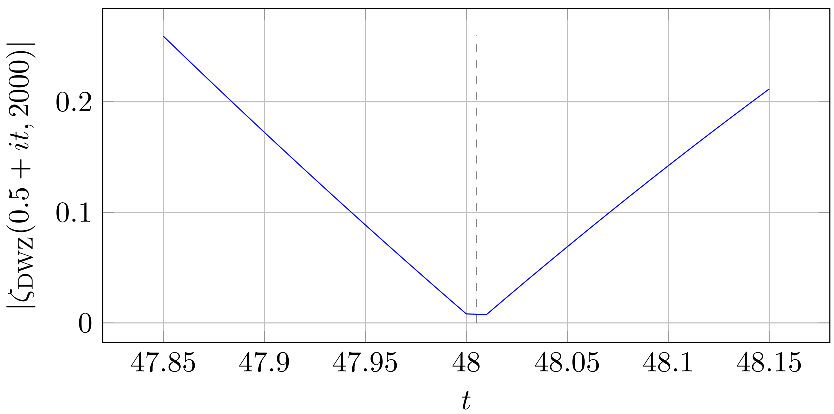

Figure 8: Scan of $|\zeta_{\mathrm{DWZ}}(0.5 + it)|$ at $W = 2000$: the candidate for zero #9 lies exactly at the minimum found, at $t \approx 48.005$.

3.4 Hardening and Pattern Hypothesis

The hybrid method was repeated for #13–#41 (29 cases): in all 29 cases, the point found agreed, within the numerical tolerance, with a known reference zero, but only in 10 cases with the exact one targeted – the remaining cases hit a neighboring zero, caused by the zero spacing shrinking with t (on average $2\pi/\ln(t/2\pi)$).

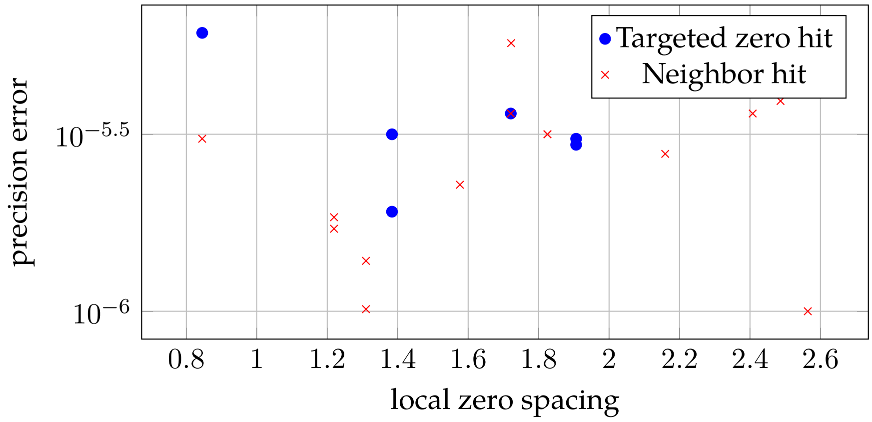

Figure 9: 20 of 29 hardening runs (the remaining 9 followed an identical pattern and are not shown individually for space reasons; the correlation below was computed over all 29): no discernible linear relationship between local zero spacing and hit rate ($r = 0.055$ over all 29).

A hypothesis derived from this ("smaller spacing ⇒ more confusions") was tested against this sample ($n = 29$). The binary outcome (targeted zero hit vs. neighbor hit) was checked here, as a simplification, against the Pearson coefficient ($r = 0.055$); a point-biserial correlation or logistic regression would be methodologically more appropriate. In the sample examined, no discernible linear relationship was found; given the limited sample size and in the absence of a reported p-value, no general exclusion of a relationship is derived from this – only that this sample provides no evidence for one.

3.5 Numerical Reproduction and Reference Check for 25 Zeros

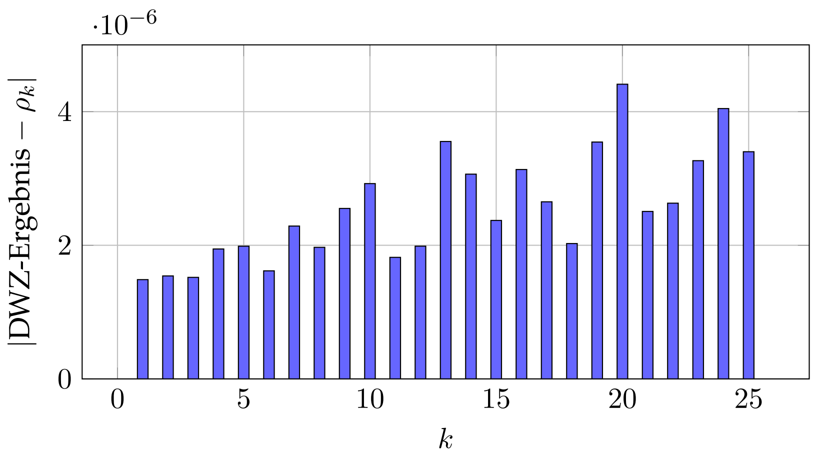

Figure 10: Absolute position deviation $e_k^{(M_1)}(W{=}10^4)$ for all 25 zeros: consistently between 1.5×10^{-6} and 4.4×10^{-6}, with no trend as k increases.

Table 10: DWZ method: deviation from the reference position for $k = 1, \ldots, 25$.

k	$t = \mathrm{Im}(\rho_k)$	$\lvert$DWZ result $- \rho_k\rvert$
1	14.1347	1.49×10^{-6}
2	21.0220	1.54×10^{-6}
3	25.0109	1.52×10^{-6}
4	30.4249	1.95×10^{-6}
5	32.9351	1.99×10^{-6}
6	37.5862	1.62×10^{-6}
7	40.9187	2.29×10^{-6}
8	43.3271	1.97×10^{-6}
9	48.0052	2.55×10^{-6}
10	49.7738	2.92×10^{-6}
11	52.9703	1.82×10^{-6}
12	56.4462	1.99×10^{-6}
13	59.3470	3.55×10^{-6}
14	60.8318	3.07×10^{-6}
15	65.1125	2.37×10^{-6}
16	67.0798	3.13×10^{-6}
17	69.5464	2.65×10^{-6}
18	72.0672	2.03×10^{-6}
19	75.7047	3.55×10^{-6}
20	77.1448	4.41×10^{-6}
21	79.3374	2.51×10^{-6}
22	82.9104	2.63×10^{-6}
23	84.7355	3.27×10^{-6}
24	87.4253	4.05×10^{-6}
25	88.8091	3.40×10^{-6}
Minimum / mean / maximum		1.49 / 2.57 / 4.41 $(\times 10^{-6})$

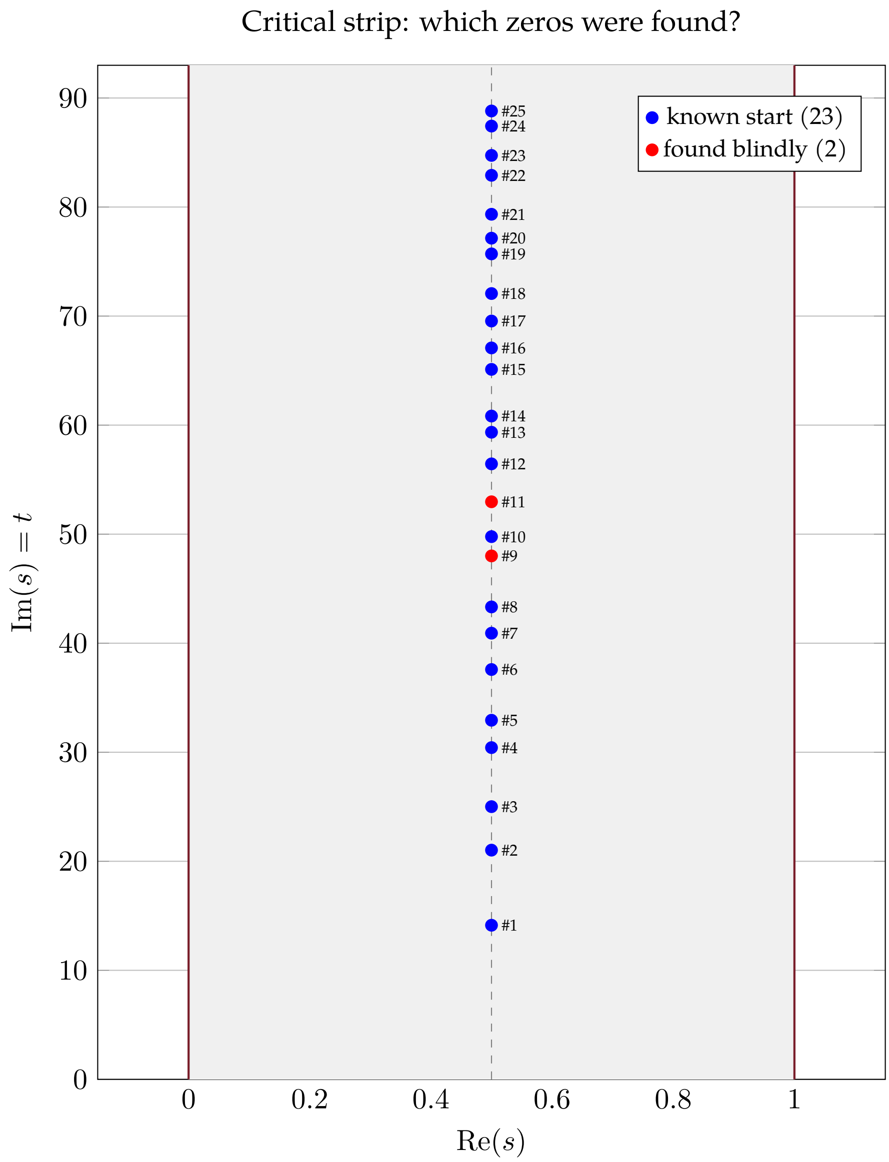

Figure 11: Critical strip $0 < \mathrm{Re}(s) < 1$ (gray) with all 25 zeros numerically reproduced by the DWZ method (Table 10): blue = used as the known reference position for Newton refinement (23), red = found blindly, without prior knowledge of the exact position (2, #9 and #11) – $8\,\%$ of the total. For all 25, the result agrees with the reference to within 1.5–4.4×10^{-6}, regardless of the method used to find it (no point is unaccounted for). The additional hardening on 29 further zeros (#13–#41, Section 3) is not shown here.

3.6 Gap Verification

For nine neighboring pairs of zeros, $|\zeta_{\mathrm{DWZ}}(\frac{1}{2}+it, W{=}2000)|$ was sampled finely between the known positions (Table 11). In none of the nine intervals was an additional candidate with a sufficiently small ζ_{DWZ} magnitude observed on the chosen grid. This numerical check only shows that, on the critical line and within the grid used, no further candidate became visible – it is not a rigorous completeness proof: a zero between two grid points, a minimum shifted by finite W, or zeros away from the critical line are not thereby ruled out. Such a proof would require, for instance, an argument-principle count or a certified Turing-style zero count.

Table 11: Tested gaps between neighboring zeros.

Pair	Spacing	Result
#1–#2	6.89	no additional zero
#2–#3	3.99	no additional zero
#3–#4	5.41	no additional zero
#4–#5	2.51	no additional zero
#5–#6	4.65	no additional zero
#6–#7	3.33	no additional zero
#7–#8	2.41	no additional zero
#22–#23	1.83	no additional zero
#23–#24	2.69	no additional zero

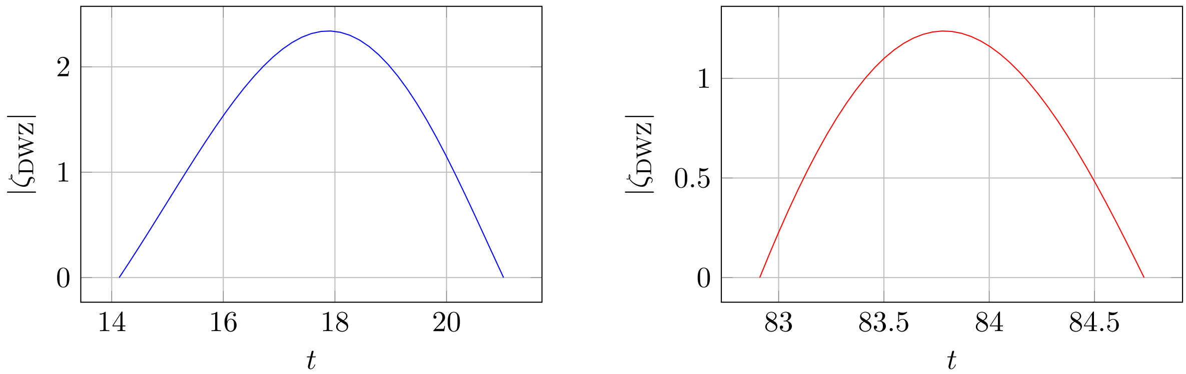

Figure 12: Two examples: largest tested spacing (#1–#2, left, spacing 6.89) and narrowest tested spacing (#22–#23, right, spacing 1.83) – in both cases only a single hump with one minimum at each edge, no hidden zero.

4 Discussion

The numerical reproduction of known zeros is a *validity demonstration of the method*, not a contribution to the Riemann Hypothesis itself. The reference values come from `mpmath` (Section 2); the DWZ method confirms that a controlled, finite width reconstruction is able to reproduce these positions with high, consistent accuracy – even where zeros lie close together.

Of the 25 zeros treated in Table 10, 2 (#9, #11) were found blindly, without prior knowledge of the exact position (8 % of the total); the remaining 23 were refined by Newton's method starting from the known reference position. The separate hardening on 29 further zeros (#13–#41) via the hybrid method at the same time reveals a real limitation of the simple hybrid search: as the zero spacing shrinks, the risk increases of hitting a neighboring zero instead of the one targeted. This limitation concerns *index assignment*, not the existence of the zeros found – all 29 hits agreed, within the stated numerical tolerance, with known reference zeros.

5 Conclusion and Outlook

The original naive definition is disproven in the critical strip (divergent). The DWZ method (Euler-Maclaurin correction) demonstrably resolves this problem, and does so considerably more efficiently than the eta-based alternative. The DRCC inequality $0 < d_{\mathrm{rec}}(X) \leq W < \infty$ was developed from an abstract condition into a concrete, data-supported formula. Open points for future work:

- A more robust fit of $C(t)$ over 50–100 zeros, to clarify the functional form (linear vs. sublinear/logarithmic); it should also be examined whether the scaling observed here (Table 8, $n = 8$) also holds outside the tested numerical range ($t \lesssim 90$ resp. $t \approx 1000$–1123).
- Adaptive scan window width (proportional to $2\pi/\ln(t/2\pi)$), to avoid the index confusion observed during hardening.
- Connecting $d_{\mathrm{rec}}(t, \varepsilon)$ to the Riemann-Siegel formula for very large $\mathrm{Im}(s)$.
- A stricter analytic error bound for $E_p(W)$ via the remainder terms of the explicit formula.

Appendix A: List of Symbols

Symbol	Meaning	First Use
s	complex variable, $s = \sigma + it$	§1.1
t	imaginary part of s ("height")	§1.1
σ	real part of s, $\sigma = \mathrm{Re}(s)$	§1.1
$\zeta(s)$	Riemann zeta function	Eq. (1)
ρ, ρ_k	nontrivial zero resp. k-th reference zero, $\rho_k = \frac{1}{2} + it_k$ (`mp.zetazero(k)`)	Eq. (3), §2.6
RH	Riemann Hypothesis (open conjecture, not proven here)	Eq. (3)
X	abstract DRCC object (here: the zeta function with its infinite sum)	§1.2
$d_{\mathrm{rec}}(X)$, $d_{\mathrm{frag}}(X)$	reconstruction resp. fragmentation degree of the abstract DRCC stability condition [7]	Eq. (4)
W, W_{trunc}	width resp. numerical truncation depth (number of summed series terms)	§1.2, Eq. (5)
$\zeta_{\mathrm{W}}(s, W)$	naive partial sum $\sum_{n=1}^{W} n^{-s}$	Eq. (5)
$\zeta_{\mathrm{DWZ}}(s, W)$	DWZ function, Variant A, model M_1 (1st-order Euler-Maclaurin)	Eq. (7)
$\eta_{\mathrm{W}}(s, W)$, $\zeta^{\eta}_{\mathrm{W}}(s, W)$	Dirichlet eta partial sum resp. Variant B	§2.3
$\zeta^{(2)}_{\mathrm{DWZ}}(s, W)$	Variant C, model M_2 (2nd-order Euler-Maclaurin)	Eq. (9)
B_2	Bernoulli number, $B_2 = 1/6$	§2.4
M, M_1, M_2	reconstruction model in general resp. Variant A / Variant C	§2.4–2.5
ω	summation order (Test A, order invariance)	§2.5
ω_{CPR}	CPR-Width (*Controlled Partial Reconstruction Width*, Hesamiy [7], external, not identified with W_{trunc})	§1.3, §2.5
$\varepsilon_{\mathrm{rec}}$	CPR-Width tolerance parameter (Hesamiy [7], external)	Table 1
ε	accuracy/tolerance threshold	Eq. (10)
$W_{\min}(M; s, \varepsilon)$	smallest width (found on the grid) that achieves ε for model M	Eq. (10)
$W^*_{\min}(s, \varepsilon)$	minimum of $W_{\min}(M; s, \varepsilon)$ over admissible models $\mathfrak{M}_{\mathrm{adm}}$	Eq. (12)
$d_{\mathrm{rec}}(t, \varepsilon)$	exact, integer reconstruction width (definition)	Eq. (13)
$\widehat{d}_{\mathrm{rec}}(t, \varepsilon)$	empirical estimator for $d_{\mathrm{rec}}(t, \varepsilon)$	Eq. (14)
$C(t)$, p	fit coefficient resp. exponent of the empirical power law $e_k(W) \approx C(t_k)W^{-p}$	Eq. (14), Table 8
$s^{(M)}_k(W)$	zero numerically determined by model M and width W, assigned to ρ_k	§2.6
$e^{(M)}_k(W)$	position error $\lvert s^{(M)}_k(W) - \rho_k \rvert$	§2.6
$E_\zeta(s, W)$	function-value error $\lvert \zeta_M(s, W) - \zeta(s) \rvert$	§2.6
$N(T)$	Riemann-von Mangoldt counting function (analytic height estimate)	Eq. (15)

Continued on next page

Appendix A: List of Symbols (continued)

Symbol	Meaning	First Use
r	Pearson correlation coefficient (pattern-hypothesis test, hardening)	§3.4
$E_p(W)$	prime-related reconstruction error (mentioned in the outlook, not formally derived in this work)	§5

References

[1] B. Riemann, *Über die Anzahl der Primzahlen unter einer gegebenen Grösse*, Monatsberichte der Berliner Akademie, 1859.

[2] E. C. Titchmarsh, *The Theory of the Riemann Zeta-Function*, 2nd ed., rev. D. R. Heath-Brown, Oxford University Press, 1986.

[3] H. M. Edwards, *Riemann's Zeta Function*, Academic Press, 1974.

[4] A. M. Turing, *Some calculations of the Riemann zeta-function*, Proc. London Math. Soc. (3) 3, 1953, pp. 99–117.

[5] A. M. Odlyzko, *Tables of zeros of the Riemann zeta function*, available at `https://www.dtc.umn.edu/~odlyzko/zeta_tables/`.

[6] F. Johansson et al., *mpmath: a Python library for arbitrary-precision floating-point arithmetic*, `http://mpmath.org`.

[7] R. Hesamiy, *DRCC: Dimensional Reduction via Controlled Combinatorics*, Munich, Germany, 2026.

[8] M. Rubinstein, *Computational methods and experiments in analytic number theory*, in: Recent Perspectives in Random Matrix Theory and Number Theory, London Math. Soc. Lecture Note Series 322, Cambridge University Press, 2005, pp. 425–506.